inorganics

MDPI

Article

A Computational Characterization of $CH_4@C_{60}$

Zdeněk Slanina [1,2,*], Filip Uhlík [3], Takeshi Akasaka [2], Xing Lu [2] and Ludwik Adamowicz [1]

[1] Department of Chemistry and Biochemistry, University of Arizona, Tucson, AZ 85721-0041, USA
[2] State Key Laboratory of Materials Processing and Die & Mould Technology, School of Material, Science and Engineering, Huazhong University of Science and Technology, Wuhan 430074, China
[3] Department of Physical and Macromolecular Chemistry, Faculty of Science, Charles University in Prague, Albertov 6, 128 43 Praha 2, Czech Republic
* Correspondence: zdeneks@email.arizona.edu

Abstract: The recently synthetically prepared endohedral $CH_4@C_{60}$ was characterized here using calculations—namely its structure, energetics, thermodynamics, and vibrational spectrum. The calculations were carried out with DFT (density-functional theory) methods, namely by the DFT M06-2X functional and MP2, as well as B2PLYPD advanced correlated, treatments with the standard 6-31++G** and 6-311++G** basis sets, corrected for the basis set superposition error evaluated using the approximative Boys–Bernardi counterpoise method. The symmetry of the endohedral obtained in the geometry optimizations was tetrahedral T. The energetics of CH_4 encapsulation into C_{60} was attractive (i.e., with a negative encapsulation-energy term), producing a substantial energy gain of −13.94 kcal/mol at the most advanced computational level, B2PLYPD/6-311++G**. The encapsulation equilibrium constants for $CH_4@C_{60}$ were somewhat higher than previously found with the $CO@C_{60}$ system. For example at 500 K, the encapsulation equilibrium constant for $CH_4@C_{60}$ had a value one order of magnitude larger than for $CO@C_{60}$. The encapsulation thermodynamic characteristics suggest that high-pressure and high-temperature synthesis could in principle also be possible for $CH_4@C_{60}$.

Keywords: metallic and non-metallic endohedrals; fullerene encapsulation; stability calculations; theory–experiment comparison

Citation: Slanina, Z.; Uhlík, F.; Akasaka, T.; Lu, X.; Adamowicz, L. A Computational Characterization of $CH_4@C_{60}$. *Inorganics* **2024**, *12*, 64. https://doi.org/10.3390/inorganics12030064

Academic Editor: Michael A. Beckett

Received: 11 January 2024
Revised: 5 February 2024
Accepted: 17 February 2024
Published: 21 February 2024

1. Introduction

Fullerenes can encapsulate not only single metals and their aggregates but also non-metals and their molecules. Thus, species like $N_2@C_{60}$, $CO@C_{60}$, and $N_2@C_{70}$ have been produced [1], namely by application of high pressures at high temperatures. Moreover, $N_2@C_{60}$ can also be prepared [2,3] by implantation of the nitrogen ion into the C_{60} cage, though this technique is preferentially used for the preparation of $N@C_{60}$ [2–9]. Other non-metallic endohedrals encapsulate noble-gas atoms [10–14], again produced [10] by high pressures at high temperatures and with the help of catalytic action [13]. Moreover, with an entirely different method, an ingenious synthetic approach, hydrogen molecules [15] or even water [16] were first placed inside open fullerene cages that were subsequently closed through synthetic steps [17,18]. More recently, such elegant treatments even enabled [19] preparation of $(H_2O)_2@C_{70}$. Similarly, carbon monoxide [20,21] as well as hydrogen peroxide [22,23] were also deposited inside derivatives of open C_{60} cage. Such fullerene encapsulations of non-metals have also been calculated, for example in works [24–35] (for a survey, see ref. [36] and references therein) with the first calculations [24] dating from the year 1991. These calculations mostly deal with encapsulations in the C_{60} cage; however, C_{70} and C_{84} [25,36], $C_{59}N$ [33,34], and even $C_{60}H_n$ [25] cases have also been studied.

The present report continues with the latter efforts and describes quantum chemical characterization of the structural and vibrational spectral features, encapsulation energetics, and thermodynamics of the recently prepared [37] $CH_4@C_{60}$ species.

2. Calculations

The calculation treatment started with structure optimizations carried out with a DFT (density-functional theory) approach, viz the DFT M06-2X functional considered [38] the most reliable technique for various species and aspects, including hydrogen-bonded systems and long-range interactions. The M06-2X functional was combined with the conventional 6-31++G** basis set [39] (the treatment is labeled here as M06-2X/6-31++G**). Subsequently, in the localized M06-2X/6-31++G** hypersurface stationary points, a GF (harmonic) vibrational analysis was performed, which allowed checking the nature of the stationary points; i.e., if local energy minima had really been found (and not activated complexes or even higher types of hypersurface stationary points). For numerical integration with the DFT functional, a so called ultrafine grid was applied. Moreover, the tight SCF (self-consistent field) convergency criterion was used. Finally, the wave function stability was tested throughout, in order to eliminate unstable SCF solutions lacking real physical significance.

The M06-2X/6-31++G** calculated energetics of the encapsulation process was further checked and refined by more advanced, correlated quantum chemical methods, namely by the second-order perturbation Møller-Plesset (MP2) treatment [40], considering all electrons (MP2 = FU) with the conventional 6-31++G** and 6-311++G** basis sets in the previously optimized M06-2X/6-31++G** structure. Moreover, an even more advanced and recently introduced technique known as B2PLYPD = FU [41] (again with all electrons) was also employed for refining the encapsulation energetics. The B2PLYPD technique is based on the MP2 method, however combined with the DFT approach and with inclusion of dispersion correction (D). In addition, the so-called basis set superposition error (BSSE) was also evaluated for the encapsulation energy, namely by the approximative Boys–Bernardi counterpoise method (also known as CP2) [42], since this was recently considered [43] with metallofullerenes. The Boys–Bernardi approach to the BSSE correction term is an approximative scheme that ensures that every reaction component of a studied chemical process is formally described using the same number of basis functions. The required situation is realized by rather artificial (also called ghost) atoms possessing no electrons. The BSSE issue is essentially rooted in the fact that the considered basis sets are always finite. In other words, the BSSE term would disappear in a situation with a basis set with an infinite number of basis functions (of course, such an infinite scheme cannot practically be handled). The BSSE correction term represents an important addition to the energetics of any encapsulation process—without the BSSE correction, the energy gain created by encapsulation would be exaggerated (endohedrals would be artificially over-stabilized). The molecular partition functions used in the thermodynamic treatment are approximated by the rigid rotator and harmonic oscillator (RRHO) description [36], as this treatment represents the only approach applicable to such relatively large systems with the computer resources available at present. All the reported calculations were performed with the program Gaussian 09 [44]. The calculations were carried out with computers operating in parallel regime, mostly with 8–24 processors (with a computational frequency up 3 GHz each and with available operational memory up to 60 GB).

3. Results and Discussion

The presented calculations deal with the encapsulation equilibrium process in the gas-phase:

$$CH_4(g) + C_{60}(g) = CH_4@C_{60}(g) \tag{1}$$

connected with the encapsulation change in the potential energy ΔE_{enc} and also described by the encapsulation equilibrium constant $K_{p,enc}$, defined by the partial pressures p of the individual reaction components:

$$K_{p,enc} = \frac{p_{CH_4@C_{60}}}{p_{CH_4} p_{C_{60}}}. \tag{2}$$

The equilibrium constant $K_{p,enc}$ for encapsulation (1) is related, as usual, to the standard reaction Gibbs energy change $\Delta G^o_{T,enc}$ (at a temperature T):

$$\Delta G^o_{T,enc} = -RTlnK_{p,enc} \quad (3)$$

where R denotes the gas constant. Finally, the standard encapsulation Gibbs energy change $\Delta G^o_{T,enc}$ is related to the standard change of the encapsulation enthalpy at temperature T, $\Delta H^o_{T,enc}$, as well as to the standard encapsulation entropy change $\Delta S^o_{T,enc}$ at temperature T:

$$\Delta G^o_{T,enc} = \Delta H^o_{T,enc} - \Delta T S^o_{T,enc} \, . \quad (4)$$

Both latter terms were evaluated here through a statistical mechanical treatment based on the RRHO partition functions. As these calculations deal with the species in the gas-phase, no solvent effects needed to be included.

The molecular–structure optimizations began from selected different initial arrangements for the CH_4@C_{60} complex. The optimized potential energy minimum exhibited tetrahedral T symmetry (Figure 1). The C-H bond length was only slightly influenced by the encapsulation. In the free CH_4, its calculated M06-2X/6-31++G** C-H bond length was equal to 1.091 Å while after the encapsulation, the C-H bond at the M06-2X/6-31++G** level equaled 1.088 Å. Similarly, the changes in the C-C bond lengths on the C_{60} cage were also small. The 6/6 and 5/6 C-C bond lengths for the empty C_{60} were calculated at the M06-2X/6-31++G** level as 1.388 and 1.452 Å, respectively. In the CH_4@C_{60} endohedral at the same level, the 6/6 bonds spanned an interval 1.389–1.390 Å, while for the 5/6 bonds this was 1.451–1.454 Å.

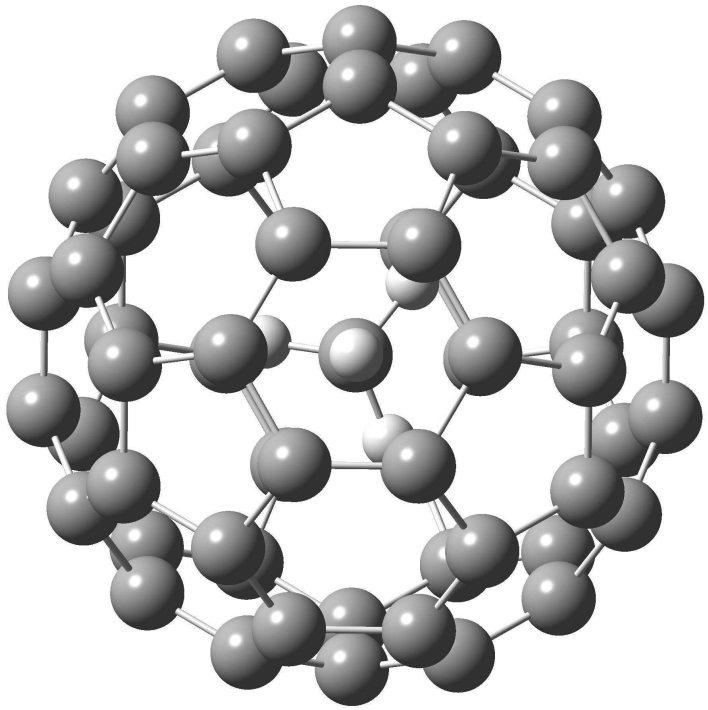

Figure 1. M06-2X/6-31++G** optimized structure of CH_4@C_{60}.

With respect to the thermodynamic evaluations, it should be mentioned that some common quantum chemical programs can erroneously work with an incorrect symmetry number for the I_h icosahedral C_{60} cage. In fact, they simply deal with a value of one instead of the proper [36] (and used here) value of sixty. Actually, the I_h symmetry number was only discussed for the first time [36] in the year 1989, soon after the discovery of C_{60}, as previously there was no usage of the term. Before C_{60} studies, only two other icosahedral molecules were known (dodecahedrane $C_{20}H_{20}$ and dodecaborate ion $B_{12}H_{12}^{2-}$). At present,

on the other hand, there is a whole series of (topological) icosahedral fullerenes, like C_{20}, C_{80}, C_{120}, C_{180}, etc., though some of them undergo Jahn–Teller conditioned symmetry reduction in quantum chemical structural optimizations; for example, C_{20} and C_{80}. The Jahn–Teller effect in such icosahedral cages can still be suppressed by the charge transfer present in metallofullerenes. Such restoration of symmetry happens, for example, in $La_2@C_{80}$ derived from the icosahedral C_{80} cage (which is actually [36] the most populated isomer of $La_2@C_{80}$—in contrast to the set of the empty C_{80} cages where the icosahedral cage is, on the contrary, the least populated).

In particular, application of a simple symmetry number of one for C_{60}, instead of the correct value of sixty, would imply a change in equilibrium constant by a huge multiplication factor of 60. Incidentally, a somewhat similar issue also appears [45] with the contribution of chirality to the partition functions; i.e., a factor equal to 2. Both issues are obviously important for thermodynamic stability evaluations. The encapsulation equilibrium constant $K_{p,enc}$ from Equation (2) can be expressed [36] by a compact formula using the molecular partition functions q_i^o (the partition functions also have to correspond to the selected standard state, i.e., here an ideal gas phase at 1 atm = 101,325 Pa pressure) and the standard encapsulation enthalpy change at absolute zero temperature $\Delta H^o_{0,enc}$:

$$K_{p,enc} = \frac{\frac{q^o_{CH_4@C_{60}}}{N_A}}{\frac{q^o_{CH_4}}{N_A}\frac{q^o_{C_{60}}}{N_A}} exp[-\frac{\Delta H^o_{0,enc}}{RT}] \,, \tag{5}$$

where the symbol N_A stands for the Avogadro number. The standard encapsulation enthalpy change at the absolute zero temperature $\Delta H^o_{0,enc}$ actually has the meaning of the ground-state energy change; i.e., it contains the encapsulation reaction change ΔZPE_{enc} in the vibrational zero-point energy (ZPE):

$$\Delta H^o_{0,enc} = \Delta E_{enc} + \Delta ZPE_{enc} \,. \tag{6}$$

Let us note that the form of formula (5) should allow some partial cancellation of higher contributions [36] beyond simple RRHO approximation like anharmonicity corrections. As for the symmetry numbers, they have their roots in the rigorous quantum mechanical requirements for the symmetry behavior of wave functions. Practically speaking, the symmetry number is equal to the number of rotations of the molecule that convert it into an identical position; hence, this is given by the order of the rotational subgroup of the related molecular point group of symmetry. The symmetry numbers appear in the rotational contributions to the molecular partition functions q_i^o in Equation (5) and can thus significantly contribute to the values of equilibrium constants.

The situation is more complex with fullerene endohedrals, as their encapsulates can exhibit rotational motions in the cages (or at least large amplitude oscillations). The internal motions can effectively recover [36,37,46–48] the original cage symmetry, especially at higher temperatures, thus simplifying the NMR patterns. The collective motions of encapsulates inside the cages yield a time-averaged equalizing environment on the NMR timescale. The aspects of symmetry are reflected in the so-called [36] free, fluctuating, or floating encapsulate model (FEM), originally developed for relative thermodynamic stabilities or populations of isomeric mono-metallofullerenes (where the calculated results consistently agreed [36] with the available observed data). In our situation, the endohedral symmetry should also be treated like the isomeric metallofullerenes, i.e., as the highest (topological) symmetry for the empty cage. Thus, we dealt here with just the dynamic symmetry of $CH_4@C_{60}$, i.e., I_h, not with its static tetrahedral symmetry T found from the geometry optimizations. The symmetry number for $CH_4@C_{60}$ (and for similar endohedrals based on C_{60}) was therefore here taken as [36] sixty (generally speaking, the RRHO and FEM treatments could in fact bracket out some bounds for thermodynamic terms). Incidentally, this treatment also removed the chirality feature of the T symmetry in this case. Obviously,

the change in the symmetry number (from 12 for T to 60 for I_h) was quite profound and the consequences for the thermodynamic stabilities were substantial.

The Mulliken charges on atoms calculated at the M06-2X/3-21G level indicated that there was a (small) negative charge transfer of −0.069 (in elementary charge units) from CH_4 to the C_{60} cage (so that there was an electrostatic contribution to the stabilization, cf. $H_2O@C_{59}N$ [33,34]). Such a rather negligible charge transfer, however, stands in clear contrast to the substantial charge transfers known [36] for metallofullerenes. Mulliken charges on the cage carbons have values between −0.007 and +0.003. The Mulliken charge on the carbon in the free CH_4 at the same level was equal to −0.787, while in the encapsulated CH_4 this amounted to −0.764 (on H atoms of the encapsulated CH_4 it was +0.208). Let us mention for completeness that the Mulliken charges on atoms, due to their historical construction, were calculated using smaller sets of basis functions, like for example the standard 3–21 G basis set used here. Mulliken charges on atoms calculated with the 3–21 G basis set are known [49] to produce a good agreement with the available observed charges [50]. In addition, there are also more general methodological reasons [51,52] why some larger basis sets should not be applied in the calculation of the Mulliken atomic charge on atoms.

Table 1 presents the encapsulation energy ΔE_{enc} for $CH_4@C_{60}$ evaluated with the four selected approaches. The ΔE_{enc} term was always negative—there was an energy gain upon the encapsulation, responsible for the complex stabilization. At the DFT M06-2X level, both considered basis sets produced about the same values. Similarly, the correlated MP2 and B2PLYPD encapsulation energies were quite close. As the B2PLYPD treatment is the most sophisticated among the four approaches considered in Table 1 (and also very close to the value in [35]), the ΔE_{enc} value of −13.94 kcal/mol was used in the subsequent evaluations of the thermodynamic stability. After the addition of the M06-2X/6-31++G** ΔZPE_{enc} term, the corresponding encapsulation enthalpy change at absolute zero temperature $\Delta H^o_{0,enc}$ amounted to −11.38 kcal/mol. The encapsulation energy ΔE_{enc} of −13.94 kcal/mol was comparable with the energy gain found in [36] for the encapsulation producing $CO@C_{60}$ (−12.5 kcal/mol) or for the encapsulation yielding [36] $N_2@C_{60}$. Moreover, $CH_4@C_{60}$ had a significantly larger energy gain than the endohedrals [36] $H_2@C_{60}$, $Ne@C_{60}$, or [36] $NH_3@C_{60}$ (though not as high as that found in [36] for $(H_2O)_2@C_{70}$, $(H_2O)_2@C_{84}$). For example, the formation of $NH_3@C_{60}$ was calculated [36] to be connected with an encapsulation energy of just −5.23 kcal/mol at the MP2 = FC/6-31G** level.

Table 1. The encapsulation energy ΔE_{enc} for $CH_4@C_{60}$ calculated with the selected approaches [a] and with inclusion of BSSE correction.

Calc. Level	ΔE_{enc} (kcal.mol $^{-1}$)
M06-2X/6-31++G**	−16.35
M06-2X/6-311++G**	−16.41
MP2/6-311++G**	−14.22
B2PLYPD/6-311++G**	−13.94

[a] In the M06-2X/6-31++G** optimized geometry, see Figure 1.

The temperature interplay between the standard change of the encapsulation enthalpy $\Delta H^o_{T,enc}$ and the standard entropy change $T\Delta S^o_{T,enc}$ yielded the encapsulation equilibrium constants $K_{p,enc}$ (Table 2). The presented $K_{p,enc}$ values were higher than those found in [36] for the $CO@C_{60}$ formation. For example, at 500 K, the encapsulation equilibrium constant $K_{p,enc}$ for CH_4 had a value of 0.0114 atm^{-1}, while in the case of $CO@C_{60}$ its value in [36] was lower by one order of magnitude, namely 0.00118 atm^{-1}. The finding suggests that production of $CH_4@C_{60}$ by applying high pressures at high temperature could in principle be possible. However, there is not only thermodynamic, but also kinetic, aspects. An efficient reaction mechanism is needed for encapsulation with high pressure at high temperature [1,7], which should temporarily open a window in the fullerene cage. In fact, a catalytic (or autocatalytic) action [13,53,54] is required for the window opening (and also

for its closure). The standard encapsulation changes in enthalpy $\Delta H^o_{T,enc}$ for process (1) consistently exhibit a negative sign. In the view of the van't Hoff relationship,

$$\frac{dlnK_{p,enc}}{dT} = \frac{\Delta H^o_{T,enc}}{RT^2} \quad (7)$$

the encapsulation equilibrium constant $K_{p,enc}$ must exhibit a decreasing course with increasing temperature—as indeed seen in both Table 2 and Figure 2.

Table 2. The standard [a] enthalpy $\Delta H^o_{T,enc}$, entropy $T\Delta S^o_{T,enc}$, Gibbs energy $\Delta G^o_{T,enc}$ changes, and the equilibrium constants $K_{p,enc}$ for the gas-phase equilibrium formation (1) of $CH_4@C_{60}$ evaluated [b] at the selected temperatures T.

T (K)	$\Delta H^o_{T,enc}$ (kcal/mol)	$T\Delta S^o_{T,enc}$ (kcal/mol)	$\Delta G^o_{T,enc}$ (kcal/mol)	$K_{p,enc}$ (atm^{-1})
298.15	−11.87	−9.82	−2.05	$3.18 \times 10^{+1}$
500	−11.29	−15.74	4.45	1.14×10^{-2}
1000	−9.47	−28.97	19.50	5.47×10^{-5}
1500	−7.58	−41.15	33.58	1.28×10^{-5}

[a] The standard state—ideal gas phase at 1 atm = 101325 Pa pressure. [b] Calculated with the B2PLYPD/6-311++G** energetics and the M06-2X/6-31++G** partition functions.

GF vibrational analysis was used here for confirmation that the energy minimum was indeed found (no imaginary frequency) and as input for the RRHO partition functions. Figure 3 shows the M06-2X/6-31++G** calculated IR and Raman harmonic vibrational spectrum of $CH_4@C_{60}$. The high I_h symmetry [55] of the free C_{60} grossly simplifies its IR vibrational spectrum [56]. The symmetry representation $\Gamma_{C_{60}}$ of the 174 vibrational modes of C_{60} was as follows [57]:

$$\Gamma_{C_{60}} = 2A_g + A_u + 3T_{1g} + 4T_{2g} + 4T_{1u} + 5T_{2u} + 6G_u + 6G_g + 8H_g + 7H_u, \quad (8)$$

where A, T, G, and H denote one-, three-, four-, and five-fold degenerate modes, respectively (so that we deal with a number of modes $3 \times 1 + 16 \times 3 + 12 \times 4 + 15 \times 5 = 174 = 60 \times 3 - 6$). This high symmetry actually led to only 46 distinct vibrational frequencies [57], with four of them (T_{1u}) active in the IR and ten of them (A_g, H_g) in the Raman spectra. However, if the high symmetry of the cage was reduced by encapsulation, the spectral symmetry selection rules should also be relaxed. Nevertheless, even the $CH_4@C_{60}$ IR spectrum primarily consisted of four (broader) bands. The CH_4 vibrational modes appeared in the $CH_4@C_{60}$ spectrum, with low intensities in the regions around 1300 cm^{-1} (the bond-angle deformation, in the free CH_4 at the M06-2X/6-31++G** level amounted to 1349 cm^{-1}) and around 3200 cm^{-1} (bond stretching, in the free CH_4 3192 cm^{-1}). The $CH_4@C_{60}$ endohedral had 189 vibrational modes—174 of them actually originated from the vibrational modes of the free C_{60} and 9 from the vibrational modes of the free CH_4, though their frequencies were somewhat shifted and the exact degeneracies had been removed. The remaining six vibrational modes had the nature of hindered rotational motions or hindered translational motions of CH_4 in the C_{60} cage (the translational motions can also be viewed as the encapsulate vibrations between the cage walls). The hindered collective motions actually possessed the lowest frequencies in the vibrational spectrum, about 173 cm^{-1} for the hindered rotations and about 247 cm^{-1} for the hindered translations (though their IR intensities were negligible, while the modes around 247 cm^{-1} should have still been a bit more active in the Raman spectra). In contrast to the straightforward FEM treatment of the relative thermodynamic stabilities or populations in sets of isomeric monometallofullerenes [36], the lowest vibrational modes in our case were important for the description of the overall encapsulation thermodynamics. The six lowest vibrational

modes were also primary contributors to the encapsulation reaction change ΔZPE_{enc} of the vibrational zero-point energy in Equation (6).

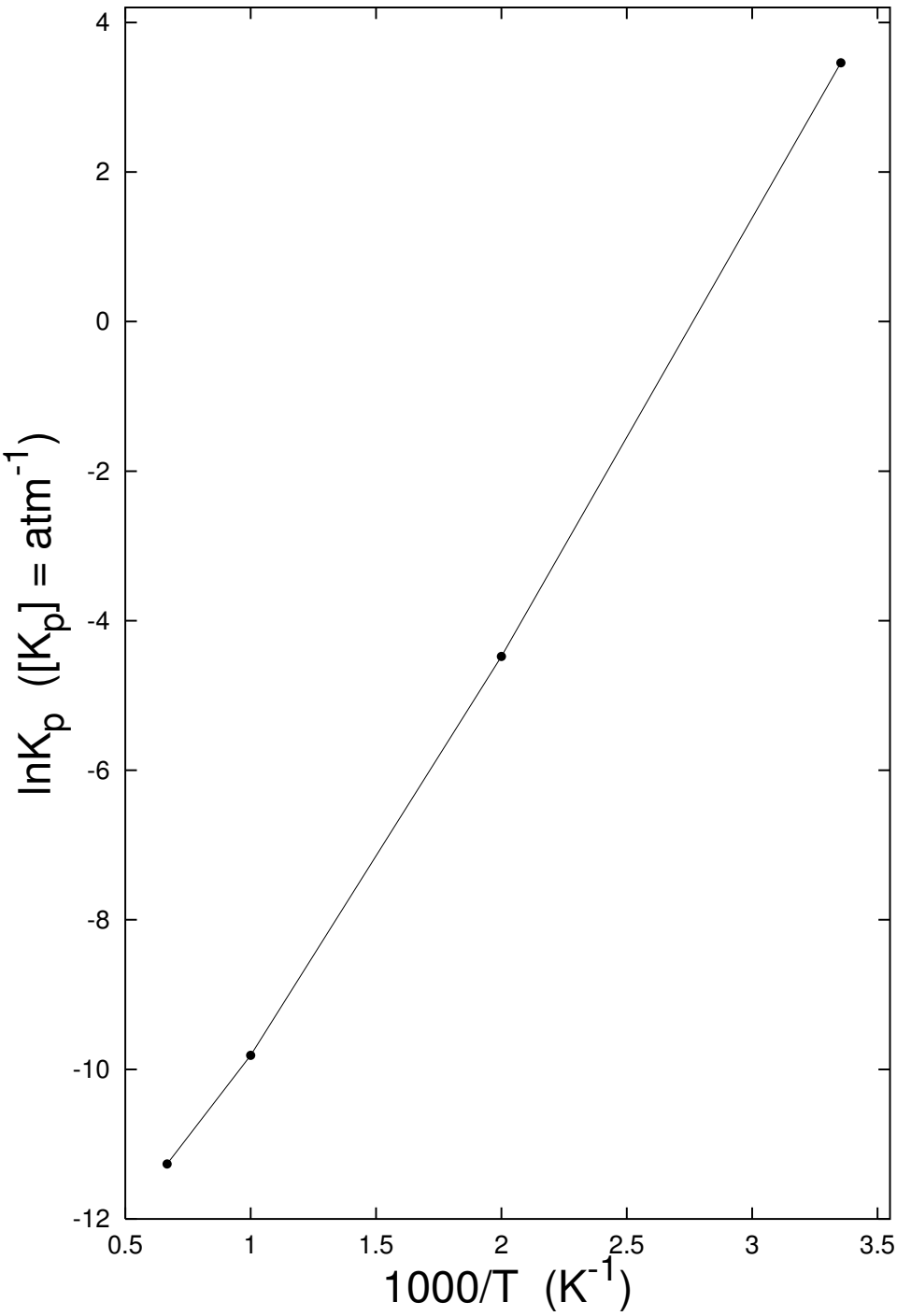

Figure 2. Temperature dependency of the equilibrium constant (2) for CH_4 encapsulation in C_{60}.

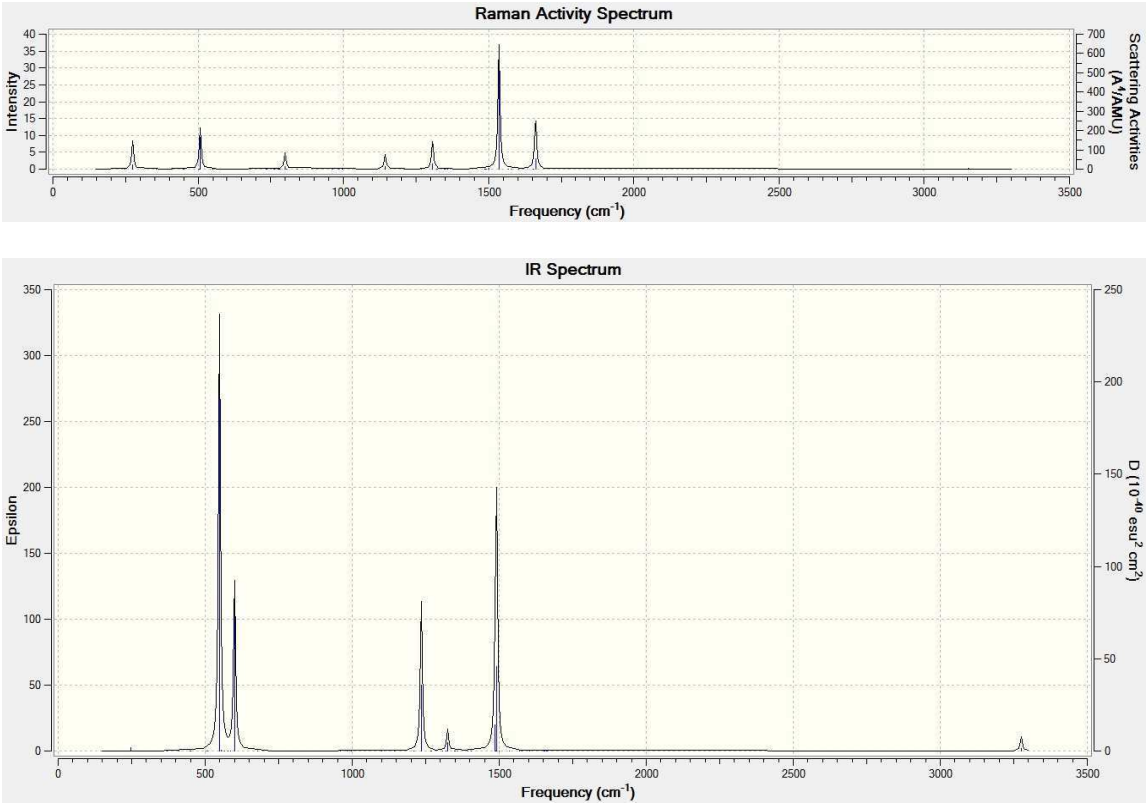

Figure 3. M06-2X/6-31++G** computed IR and Raman (top) spectrum of CH_4@C_{60}.

In addition to C_{60}, the C_{84} cages could also be of interest for the CH_4 accommodation. C_{84} is a relatively well known system of isomeric fullerenes, in particular the two most common isomers, D_2 and D_{2d}, conventionally also labeled [58] as 22 and 23, D_2(22)-C_{84} and D_{2d}(23)-C_{84}. The D_{2d} structure is the lowest-energy isomer, but it is located only about 0.5 kcal/mol below the D_2 species [59]. The M06-2X/6-31++G** water dimer encapsulation energy into the D_2(22)-C_{84} cage was calculated [36] as −17.4 kcal/mol, while for D_{2d}(23)-C_{84}, it was −14.4 kcal/mol. On the other hand, the inclusion of the water dimer into C_{60} was repulsive [26]. Incidentally, our ongoing calculations on CO_2@D_{2d}(23)-C_{84} at the M06-2X/6-31+G* level preliminary gave an encapsulation energy of −13.6 kcal/mol. Hence, CH_4@C_{84} should also be of computational interest in further studies.

In future, still higher methodological levels for the molecular structure optimization and energetics, as well as more advanced descriptions of the motions of the encapsulate in the cage, with related modifications of the RRHO approximation (including the combination [36] of the RRHO and FEM treatments), should be considered. Another more advanced approach [60] treats the motions of a monoatomic encapsulate (for example in He@C_{60}) as the quantum problem of a particle in a sphere (a similar approach [60] can also be developed for encapsulate motions in nanotubes using a model cylinder). This approach produces contributions to thermodynamic functions, showing for example an interesting temperature development [60,61] of the heat capacity. Further generalizations of this approach could lead to a more realistic description of the encapsulation thermodynamics. A generalization of the classical Pitzer description [62] of the hindered internal rotations in molecules should also be studied [55,63] for this purpose. Moreover, there have been some promising results [36] for anharmonicity considerations based on quantum chemical calculations, too. Finally, let as mention for completeness that topological, non-numerical approaches [64–67] can also be useful in understanding some encapsulation issues.

Such expected future progress should in turn encourage studies of still more complex nanocarbon systems [68–71] via applications of Gibbs energy treatments. The results of

such more advanced calculations with an even higher accuracy could also be used in the search for non-metallic fullerene endohedrals in the interstellar spectra (diffuse interstellar bands, DIBs). This would be a subsequent step after the discovery [72–74] of the empty C_{60} and C_{70} in interstellar space and hypotheses [75–77] of their origin there. One of the possible endohedral candidates is [78] $H_2O@C_{60}^{+}$. For the application, the calculations should also be adjusted for charged species (including electronic spectra).

4. Conclusions

The previously synthetically prepared endohedral $CH_4@C_{60}$ was characterized through calculations. The symmetry of the endohedral was found to be tetrahedral T symmetry. The calculated encapsulation energetics were attractive, with a substantial energy gain of −13.94 kcal/mol at the most advanced computational level. The encapsulation equilibrium constants for $CH_4@C_{60}$ were somewhat higher than previously found with the $CO@C_{60}$ system—this finding suggests that high-pressure and high-temperature synthesis could in principle be possible for $CH_4@C_{60}$. In future, these computational approaches should be developed further, for both encapsulation energetics and description of the motions of the encapsulate in the cage. The presented results encourage studies of still more complex endohedral and other nanocarbon systems.

Author Contributions: Conceptualization, Z.S., T.A. and X.L.; methodology, Z.S. and L.A.; hardware and software, Z.S., F.U. and L.A.; models validation, Z.S., T.A., X.L. and L.A.; analysis and interpretation, Z.S., F.U., T.A. and X.L.; writing—original draft preparation, Z.S. and F.U. All authors have read and agreed to the published version of the manuscript.

Funding: The reported research has been supported by the National Natural Science Foundation of China (21925104 and 92261204), the Hubei Provincial Natural Science Foundation of China (No. 2021CFA020), and the International Cooperation Key Project of Science and Technology Department of Shaanxi; and by the Charles University Centre of Advanced Materials/CUCAM (CZ 02.1.01/0.0/0.0/15_003/0000417), the MetaCentrum (LM2010005) and CERIT-SC (CZ.1.05/3.2.0-0/08.0144) computing facilities.

Data Availability Statement: The data presented in this study are available in article.

Acknowledgments: An initial phase of the research line was supported by the Alexander von Humboldt-Stiftung and the Max-Planck-Institut für Chemie (Otto-Hahn-Institut).

Conflicts of Interest: The authors declare no conflict of interest.

References

1. Peres, T.; Cao, B.P.; Cui, W.D.; Khong, A.; Cross, R.J.; Saunders, M.; Lifshitz, C. Some new diatomic molecule containing endohedral fullerenes. *Int. J. Mass Spectr.* **2001**, *210/211*, 241–247. [CrossRef]
2. Suetsuna, T.; Dragoe, N.; Harneit, W.; Weidinger, A.; Shimotani, H.; Ito, S.; Takagi, H.; Kitazawa, K. Separation of $N_2@C_{60}$ and $N@C_{60}$. *Chem. Eur. J.* **2002**, *8*, 5079–5083. [CrossRef] [PubMed]
3. Suetsuna, T.; Dragoe, N.; Harneit, W.; Weidinger, A.; Shimotani, H.; Ito, S.; Takagi, H.; Kitazawa, K. Separations of $N_2@C_{60}$ and $N@C_{60}$ (vol 8, pg 5079, 2002). *Chem. Eur. J.* **2003**, *9*, 598. [CrossRef]
4. Murphy, T.A.; Pawlik, T.; Weidinger, A.; Höhne, M.; Alcala, R.; Spaeth, J.-M. Observation of atomlike nitrogen in nitrogen-implanted solid C_{60}. *Phys. Rev. Lett.* **1996**, *77*, 1075–1078. [CrossRef]
5. Knapp, C.; Dinse, K.-P.; Pietzak, B.; Waiblinger, M.; Weidinger, A. Fourier transform EPR study of $N@C_{60}$ in solution. *Chem. Phys. Lett.* **1997**, *272*, 433–437. [CrossRef]
6. Pietzak, B.; Waiblinger, M.; Murphy, T.A.; Weidinger, A.; Höhne, M.; Dietel, E.; Hirsch, A. Buckminsterfullerene C_{60}: A chemical Faraday cage for atomic nitrogen. *Chem. Phys. Lett.* **1997**, *279*, 259–263. [CrossRef]
7. Cao, B.P.; Peres, T.; Cross, R.J.; Saunders, M.; Lifshitz, C. Do nitrogen-atom-containing endohedral fullerenes undergo the shrink-wrap mechanism? *J. Phys. Chem. A* **2001**, *105*, 2142–2146. [CrossRef]
8. Kobayashi, K.; Nagase, S.; Dinse, K.-P. A theoretical study of spin density distributions and isotropic hyperfine couplings of N and P atoms in $N@C_{60}$, $P@C_{60}$, $N@C_{70}$, $N@C_{60}(CH_2)_6$, and $N@C_{60}(SiH_2)_6$. *Chem. Phys. Lett.* **2003**, *377*, 93–98. [CrossRef]
9. Wakahara, T.; Matsunaga, Y.; Katayama, A.; Maeda, Y.; Kako, M.; Akasaka, T.; Okamura, M.; Kato, T.; Choe, Y.K.; Kobayashi, K.; et al. A comparison of the photochemical reactivity of $N@C_{60}$ and C_{60}: Photolysis with disilirane. *Chem. Commun.* **2003**, *39*, 2940–2941. [CrossRef]

10. Saunders, M.; Jiménez-Vázquez, H.A.; Cross, R.J.; Poreda, R.J. Stable compounds of helium and neon: He@C_{60} and Ne@C_{60}. *Science* **1993**, *259*, 1428–1430. [CrossRef] [PubMed]
11. Saunders, M.; Jiménez-Vázquez, H.A.; Cross, R.J.; Mroczkowski, S.; Freedberg, D.I.; Anet, F.A.L. Probing the interior of fullerenes by ^{3}He NMR spectroscopy of endohedral ^{3}He@C_{60} and ^{3}He@C_{70}. *Nature* **1994**, *367*, 256–258. [CrossRef]
12. Cross, R.J.; Saunders, M.; Prinzbach, H. Putting helium inside dodecahedrane. *Org. Lett.* **1999**, *1*, 1479–1481. [CrossRef]
13. Cross, R.J.; Saunders, M. Catalyzed incorporation of nobel gases in fullerenes. In *Recent Advances in the Chemistry and Physics of Fullerenes and Related Materials, Volume 11—Fullerenes for the New Millennium*; Kadish, K.M., Kamat, P.V., Guldi, D., Eds.; The Electrochemical Society: Pennington, NJ, USA, 2001; pp. 298–300.
14. Rubin, Y.; Jarrosson, T.; Wang, G.-W.; Bartberger, M.D.; Houk, K.N.; Schick, G.; Saunders, M.; Cross, R.J. Insertion of helium and molecular hydrogen through the orifice of an open fullerene. *Angew. Chem. Int. Ed. Engl.* **2001**, *40*, 1543–1546. [CrossRef]
15. Carravetta, M.; Murata, Y.; Murata, M.; Heinmaa, I.; Stern, R.; Tontcheva, A.; Samoson, A.; Rubin, Y.; Komatsu, K.; Levitt, M.H. Solid-state NMR spectroscopy of molecular hydrogen trapped inside an open-cage fullerene. *J. Am. Chem. Soc.* **2004**, *126*, 4092–4093. [CrossRef]
16. Iwamatsu, S.-I.; Uozaki, T.; Kobayashi, K.; Re, S.; Nagase, S.; Murata, S. A bowl-shaped fullerene encapsulates a water into the cage. *J. Am. Chem. Soc.* **2004**, *126*, 2668–2669. [CrossRef] [PubMed]
17. Komatsu, K.; Murata, M.; Murata, Y. Encapsulation of molecular hydrogen in fullerene C_{60} by organic synthesis. *Science* **2005**, *307*, 238–240. [CrossRef] [PubMed]
18. Kurotobi, K.; Murata, Y. A Single molecule of water encapsulated in fullerene C_{60}. Science **2011**, *333*, 613–616. [CrossRef]
19. Zhang, R.; Murata, M.; Aharen, T.; Wakamiya, A.; Shimoaka, T.; Hasegawa, T.; Murata, Y. Synthesis of a distinct water dimer inside fullerene C_{70}. *Nat. Chem.* **2016**, *8*, 435–441. [CrossRef] [PubMed]
20. Iwamatsu, S.; Stanisky, C.M.; Cross, R.J.; Saunders, M.; Mizorogi, N.; Nagase, S.; Murata, S. Carbon monoxide inside an open-cage fullerene. *Angew. Chem. Intl. Ed.* **2006**, *45*, 5337–5340. [CrossRef] [PubMed]
21. Shi, L.J.; Yang, D.Z.; Colombo, F.; Yu, Y.M.; Zhang, W.X.; Gan, L.B. Punching a carbon atom of C_{60} into its own cavity to form an endohedral complex CO@$C_{59}O_6$ under mild conditions. *Chem. Eur. J.* **2013**, *19*, 16545–16549. [CrossRef] [PubMed]
22. Li, Y.; Lou, N.; Xu, D.; Pan, C.; Lu, X.; Gan, L. Oxygen-delivery materials: Synthesis of an open-cage fullerene derivative suitable for encapsulation of H_2O_2 and O_2. *Angew. Chem. Int. Ed.* **2018**, *57*, 14144–14148. [CrossRef]
23. Gan, L. Molecular containers derived from [60] fullerene through peroxide chemistry. *Acc. Chem. Res.* **2019**, *52*, 1793–1801. [CrossRef] [PubMed]
24. Cioslowski, J. Endohedral chemistry: Electronic structures of molecules trapped inside the C_{60} cage. *J. Am. Chem. Soc.* **1991**, *113*, 4139–4141. [CrossRef]
25. Charkin, O.P.; Klimenko, N.M.; Charkin, D.O.; Mebel, A.M. Theoretical study of host-guest interaction in model endohedral fullerenes with tetrahedral molecules and ions of MH4 hydrides inside the $C_{60}H_{36}$, $C_{60}H_{24}$, C_{84}, and C_{60} cages. *Russ. J. Inorg. Chem.* **2004**, *49*, 868–880.
26. Ramachandran, C.N.; Sathyamurthy, N. Water clusters in a confined nonpolar environment. *Chem. Phys. Lett.* **2005**, *410*, 348–351. [CrossRef]
27. Shameema, O.; Ramachandran, C.N.; Sathyamurthy, N. Blue shift in X-H stretching frequency of molecules due to confinement. *J. Phys. Chem. A* **2006**, *110*, 2–4. [CrossRef] [PubMed]
28. Mazurek, A.P.; Sadlej-Sosnowska, N. Is fullerene C_{60} large enough to host an aromatic molecule? *Int. J. Quantum Chem.* **2011**, *111*, 2398–2405. [CrossRef]
29. Rodríguez-Fortea, A.; Balch, A.L.; Poblet, J.M. Endohedral metallofullerenes: A unique host-guest association. *Chem. Soc. Rev.* **2011**, *40*, 3551–3563. [CrossRef]
30. Varadwaj, A.; Varadwaj, P.R. Can a single molecule of water be completely isolated within the subnano-space inside the fullerene C_{60} cage? A quantum chemical prospective. *Chem. Eur. J.* **2012**, *18*, 15345–15360. [CrossRef]
31. Farimani, A.B.; Wu, Y.B.; Aluru, N.R. Rotational motion of a single water molecule in a buckyball. *Phys. Chem. Chem. Phys.* **2013**, *15*, 17993–18000. [CrossRef]
32. Popov, A.A.; Yang, S.; Dunsch, L. Endohedral fullerenes. *Chem. Rev.* **2013**, *113*, 5989–6113. [CrossRef]
33. Hashikawa, Y.; Murata, M.; Wakamiya, A.; Murata, Y. Orientation of a water molecule: Effects on electronic nature of the $C_{59}N$ cage. *J. Org. Chem.* **2017**, *82*, 4465–4469. [CrossRef]
34. Zhu, G.-Z.; Liu, Y.; Hashikawa, Y.; Zhang, Q.-F.; Murata, Y.; Wang, L.-S. Probing the interaction between the encapsulated water molecule and the fullerene cages in $H_2O@C_{60}^-$ and $H_2O@C_{59}N^-$. *Chem. Sci.* **2018**, *9*, 5666–5671. [CrossRef]
35. Jaworski, A.; Hedin, N. Local energy decomposition analysis and molecular properties of encapsulated methane in fullerene ($CH_4@C_{60}$). *Phys. Chem. Chem. Phys.* **2021**, *23*, 21554–21567. [CrossRef]
36. Slanina, Z.; Uhlík, F.; Adamowicz, L. Theoretical predictions of fullerene stabilities. In *Handbook of Fullerene Science and Technology*; Lu, X., Akasaka, T., Slanina, Z., Eds.; Springer: Singapore, 2022; pp. 111–179.
37. Bloodworth, S.; Sitinova, G.; Alom, S.; Vidal, S.; Bacanu, G.R.; Elliott, S.J.; Light, M.E.; Herniman, J.M.; Langley, G.J.; Levitt, M.H.; et al. First synthesis and characterization of $CH_4@C_{60}$. *Angew. Chem. Int. Ed.* **2019**, *58*, 5038–5043. [CrossRef]
38. Zhao, Y.; Truhlar, D.G. The M06 suite of density functionals for main group thermochemistry, thermochemical kinetics, noncovalent interactions, excited states, and transition elements: Two new functionals and systematic testing of four M06-class functionals and 12 other functionals. *Theor. Chem. Acc.* **2008**, *120*, 215–241.

39. Ditchfield, R.; Hehre, W.J.; Pople, J.A. Self-consistent molecular-orbital methods. IX. An extended Gaussian-type basis for molecular-orbital studies of organic molecules. *J. Chem. Phys.* **1971**, *54*, 724–728. [CrossRef]
40. Moller, C.; Plesset, M.S. Note on an approximation treatment for many-electron systems. *Phys. Rev.* **1934**, *46*, 618–622. [CrossRef]
41. Schwabe, T.; Grimme, S. Double-hybrid density functionals with long-range dispersion corrections: Higher accuracy and extended applicability. *Phys. Chem. Chem. Phys.* **2007**, *9*, 3397–3406. [CrossRef] [PubMed]
42. Boys, S.F.; Bernardi, F. The calculation of small molecular interactions by the difference of separate total energies. Some procedures with reduced errors. *Mol. Phys.* **1970**, *19*, 553–566. [CrossRef]
43. Slanina, Z.; Uhlík, F.; Lee, S.-L.; Adamowicz, L.; Akasaka, T.; Nagase, S. Computed stabilities in metallofullerene series: Al@C_{82}, Sc@C_{82}, Y@C_{82}, and La@C_{82}. *Int. J. Quant. Chem.* **2011**, *111*, 2712–2718. [CrossRef]
44. Frisch, M.J.; Trucks, G.W.; Schlegel, H.B.; Scuseria, G.E.; Robb, M.A.; Cheeseman, J.R.; Scalmani, G.; Barone, V.; Mennucci, B.; Petersson, G.A.; et al. *Gaussian 09, Rev. D.01*; Gaussian Inc.: Wallingford, CT, USA, 2013.
45. Slanina, Z.; Uhlík, F.; François, J.-P.; Ōsawa, E. Thermodynamic Data Bases and Optical Isomerism. *Croat. Chem. Acta* **2000**, *73*, 1047–1055.
46. Akasaka, T.; Nagase, S.; Kobayashi, K.; Wälchli, M.; Yamamoto, K.; Funasaka, H.; Kako, M.; Hoshino, T.; Erata, T. ^{13}C and ^{139}La NMR studies of La_2@C_{80}: First evidence for circular motion of metal atoms in endohedral dimetallofullerenes. *Angew. Chem. Intl. Ed. Engl.* **1997**, *36*, 1643–1645. [CrossRef]
47. Kurihara, H.; Lu, X.; Iiduka, Y.; Mizorogi, N.; Slanina, Z.; Tsuchiya, T.; Akasaka, T.; Nagase, S. Sc_2C_2@C_{80} rather than Sc_2@C_{82}: Templated formation of unexpected C_{2v}(5)C_{82} and temperature-dependent dynamic motion of internal Sc_2C_2 cluster. *J. Am. Chem. Soc.* **2011**, *133*, 2382–2385. [CrossRef]
48. Kurihara, H.; Lu, X.; Iiduka, Y.; Nikawa, H.; Hachiya, M.; Mizorogi, N.; Slanina, Z.; Tsuchiya, T.; Nagase, S.; Akasaka, T. X-ray Structures of Sc_2C_2@C_{2n} (n = 40–42): In-depth understanding of the core-shell interplay in carbide cluster metallofullerenes. *Inorg. Chem.* **2012**, *51*, 746–750. [CrossRef]
49. Slanina, Z.; Uhlík, F.; Nagase, S.; Akasaka, T.; Adamowicz, L.; Lu, X. Eu@C_{72}: Computed comparable populations of two non-IPR isomers. *Molecules* **2017**, *22*, 1053. [CrossRef]
50. Takata, M.; Nishibori, E.; Sakata, M.; Shinohara, H. Charge density level structures of endohedral metallofullerenes determined by synchrotron radiation powder method. *New Diam. Front. Carb. Technol.* **2002**, *12*, 271–286.
51. Hehre, W.J. *A Guide to Molecular Mechanics and Quantum Chemical Calculations*; Wavefunction: Irvine, CA, USA, 2003; p. 435.
52. Jensen, F. *Introduction to Computational Chemistry*; Wiley: Chichester, UK, 2017; p. 319.
53. Slanina, Z.; Uhlík, F.; Adamowicz, L.; Lee, S.-L. Computations of the catalytic effects in the Stone-Wales fullerene isomerizations: N and CN agents. *Int. J. Quantum Chem.* **2004**, *99*, 634–639. [CrossRef]
54. Hao, Y.; Tang, Q.; Li, X.; Zhang, M.; Wan, Y.; Feng, L.; Chen, N.; Slanina, Z.; Adamowicz, L.; Uhlík, F. Isomeric Sc_2O@C_{78} related by a single-step Stone-Wales transformation: Key links in an unprecedented fullerene formation pathway. *Inorg. Chem.* **2016**, *55*, 11354–11361. [CrossRef] [PubMed]
55. Slanina, Z. Some aspects of mathematical chemistry of equilibrium and rate processes: Steps towards a completely non-empirical computer design of syntheses. *J. Mol. Struct. (Theochem)* **1989**, *185*, 217–228. [CrossRef]
56. Frum, C.I.; Engleman, R., Jr.; Hedderich, H.G.; Bernath, P.F.; Lamb, L.D.; Huffman, D.R. The infrared emission spectrum of gas-phase C_{60} (buckmisterfullerene). *Chem. Phys. Lett.* **1991**, *176*, 504–508. [CrossRef]
57. Slanina, Z.; Rudziński, J.M.; Togasi, M.; Ōsawa, E. Quantum-chemically supported vibrational analysis of giant molecules: The C_{60} and C_{70} clusters. *J. Mol. Struct. (Theochem)* **1989**, *202*, 169–176. [CrossRef]
58. Manolopoulos, D.E.; Fowler, P.W. Molecular graphs, point groups, and fullerenes. *J. Chem. Phys.* **1992**, *96*, 7603–7614. [CrossRef]
59. Bakowies, D.; Kolb, M.; Thiel, W.; Richard, S.; Ahlrichs, R.; Kappes, M.M. Quantum-chemical study of C_{84} fullerene isomers. *Chem. Phys. Lett.* **1992**, *200*, 411–417. [CrossRef]
60. Uhlík, F.; Slanina, Z.; Ōsawa, E. Thermodynamic properties of He@C_{60}. *Fullerene Sci. Technol.* **2000**, *8*, 453–460. [CrossRef]
61. Suzuki, H.; Nakano, M.; Hashikawa, Y.; Murata, Y. Rotational motion and nuclear spin interconversion of H_2O encapsulated in C_{60} appearing in the low-temperature heat capacity. *J. Phys. Chem. Lett.* **2019**, *10*, 1306–1311. [CrossRef] [PubMed]
62. Pitzer, K.S. Potential energies for rotation about single bonds. *Discuss. Faraday Soc.* **1951**, *10*, 66–73. [CrossRef]
63. Gilson, M.K.; Irikura, K.K. Symmetry mumbers for rigid, flexible, and fluxional molecules: Theory and applications. *J. Phys. Chem. B* **2010**, *114*, 16304–16317. [CrossRef] [PubMed]
64. Ōsawa, E. The evolution of the football structure for the C_{60} molecule: A retrospective. *Phil. Trans. R. Soc. Lond. A* **1993**, *343*, 1–8.
65. Slanina, Z.; Lee, S.-L.; Yu, C.-H. Computations in treating fullerenes and carbon aggregates. *Rev. Comput. Chem.* **1996**, *8*, 1–62.
66. Díaz-Tendero, S.; Alcamí, M.; Martín, F. Fullerene C_{50}: Sphericity takes over, not strain. *Chem. Phys. Lett.* **2005**, *407*, 153–158. [CrossRef]
67. Vukicevic, D.; Cataldo, F.; Ori, O.; Graovac, A. Topological efficiency of C_{66} fullerene. *Chem. Phys. Lett.* **2011**, *501*, 442–445. [CrossRef]
68. Basiuk, V.A.; Basiuk, E.V. Noncovalent complexes of I_h-C_{80} fullerene with phthalocyanines. *Fuller. Nanotub. Carbon Nanostruct.* **2018**, *26*, 69–75. [CrossRef]
69. Basiuk, V.A.; Tahuilan-Anguiano, D.E. Complexation of free-base and 3d transition metal(II) phthalocyanines with endohedral fullerene Sc_3N@C_{80}. *Chem. Phys. Lett.* **2019**, *722*, 146–152. [CrossRef]

70. Li, M.; Zhao, R.; Dang, J.; Zhao, X. Theoretical study on the stabilities, electronic structures, and reaction and formation mechanisms of fullerenes and endohedral metallofullerenes. *Coor. Chem. Rev.* **2022**, *471*, 214762-1–214762-12. [CrossRef]
71. Li, Y.B.; Biswas, R.; Kopcha, W.P.; Dubroca, T.; Abella, L.; Sun, Y.; Crichton, R.A.; Rathnam, C.; Yang, L.T.; Yeh, Y.W.; et al. Structurally defined water-soluble metallofullerene derivatives towards biomedical applications. *Angew. Chem. Int. Ed. Engl.* **2023**, *62*, e202211704-1–e202211704-10.
72. Cami, J.; Bernard-Salas, J.; Peeters, E.; Malek, S.E. Detection of C_{60} and C_{70} in a young planetary nebula. *Science* **2010**, *329*, 1180–1182. [CrossRef]
73. Campbell, E.K.; Holz, M.; Gerlich, D.; Maier, J.P. Laboratory confirmation of C_{60^+} as the carrier of two diffuse interstellar bands. *Nature* **2015**, *523*, 322–323. [CrossRef]
74. Hansen, C.S.; Peeters, E.; Cami, J.; Schmidt, T.W. Open questions on carbon-based molecules in space. *Commun. Chem.* **2022**, *5*, 94-1–94-4. [CrossRef]
75. Berné, O.; Tielens, A.G.G.M. Formation of buckminsterfullerene (C_{60}) in interstellar space. *Proc. Natl. Acad. Sci. USA* **2012**, *109*, 401–406. [CrossRef]
76. Berné, O.; Montillaud, J.; Joblin, C. Top-down formation of fullerenes in the interstellar medium. *Astronom. Astrophys.* **2015**, *577*, A133-1–A133-9. [CrossRef] [PubMed]
77. Berné, O.; Montillaud, J.; Joblin, C. Top-down formation of fullerenes in the interstellar medium (Corrigendum). *Astronom. Astrophys.* **2016**, *588*, C1-1. [CrossRef]
78. Rademacher, J.; Reedy, E.S.; Negri, F.; Alom, S.; Whitby, R.J.; Levitt, M.H.; Campbell, E.K. Gas-phase electronic spectroscopy of nuclear spin isomer separated $H_2O@C_{60}^+$ and $D_2O@C_{60}^+$. *Mol. Phys.* **2023**, *122*, e2173507-1–e2173507-11.